Near-infrared coherent perfect absorption in plasmonic metal-insulator-metal waveguide

Hyeonsoo Park,[1] Seong-Yeol Lee,[1] Joonsoo Kim,[1] Byoungho Lee,[1] and Hwi Kim,[2,*]

[1]*National Creative Research Center for Active Plasmonics Application Systems, Inter-University Semiconductor Research Center and School of Electrical Engineering, Seoul National University, Gwanak-Gu Gwanakro 1, Seoul 151-742, South Korea*

[2]*Department of Electronics and Information Engineering, Korea University, 2511 Sejong-ro, Sejong 339-700, South Korea*

[*]*hwikim@korea.ac.kr*

Abstract: We propose a design of ultra-compact plasmonic coherent perfect absorber (CPA) working in the near-infrared band. The main operating mechanism is the magnetic-dipole resonant coherent absorption in the metal-insulator-metal waveguide, which enables the CPA in the near-infrared band and can be also flexibly adjusted to place the magnetic-dipole resonance at any position in the near-infrared band. Numerical analysis verifies our proposal that the magnetic resonant CPA is crucial for near-IR CPA in the ultra-compact metal-insulator-metal waveguide.

OCIS codes: (250.5403) Plasmonics; (050.6624) Subwavelength structures; (300.0300) Spectroscopy; (060.5060) Phase modulation; (230.7380) Waveguides, channeled.

References and Links

1. R. Yu, Q. Lin, S.-F. Leung, and Z. Fan, "Nanomaterials and nanostructures for efficient light absorption and photovoltaics," Nano Energy **1**(1), 57–72 (2012).
2. H. A. Atwater and A. Polman, "Plasmonics for improved photovoltaic devices," Nat. Mater. **9**(3), 205–213 (2010).
3. N. Liu, M. Mesch, T. Weiss, M. Hentschel, and H. Giessen, "Infrared perfect absorber and its application as plasmonic sensor," Nano Lett. **10**(7), 2342–2348 (2010).
4. K. Aydin, V. E. Ferry, R. M. Briggs, and H. A. Atwater, "Broadband polarization-independent resonant light absorption using ultrathin plasmonic super absorbers," Nat. Commun. **2**, 517 (2011).
5. M. K. Hedayati, M. Javaherirahim, B. Mozooni, R. Abdelaziz, A. Tavassolizadeh, V. S. K. Chakravadhanula, V. Zaporojtchenko, T. Strunkus, F. Faupel, and M. Elbahri, "Design of a perfect black absorber at visible frequencies using plasmonic metamaterials," Adv. Mater. **23**(45), 5410–5414 (2011).
6. J. Park, J.-H. Kang, A. P. Vasudev, D. T. Schoen, H. Kim, E. Hasman, and M. L. Brongersma, "Omnidirectional near-unity absorption in an ultrathin planar semiconductor layer on a metal substrate," ACS Photonics **1**(9), 812–821 (2014).
7. W. Wan, Y. Chong, L. Ge, H. Noh, A. D. Stone, and H. Cao, "Time-reversed lasing and interferometric control of absorption," Science **331**(6019), 889–892 (2011).
8. Y. D. Chong, L. Ge, H. Cao, and A. D. Stone, "Coherent perfect absorbers: time-reversed lasers," Phys. Rev. Lett. **105**(5), 053901 (2010).
9. J. Zhang, K. F. MacDonald, and N. I. Zheludev, "Controlling light-with-light without nonlinearity," Light Sci. Appl. **1**(7), e18 (2012).
10. M. Pu, Q. Feng, M. Wang, C. Hu, C. Huang, X. Ma, Z. Zhao, C. Wang, and X. Luo, "Ultrathin broadband nearly perfect absorber with symmetrical coherent illumination," Opt. Express **20**(3), 2246–2254 (2012).
11. S. Huang and G. S. Agarwal, "Coherent perfect absorption of path entangled single photons," Opt. Express **22**(17), 20936–20947 (2014).
12. N. Gutman, A. A. Sukhorukov, Y. D. Chong, and C. M. de Sterke, "Coherent perfect absorption and reflection in slow-light waveguides," Opt. Lett. **38**(23), 4970–4973 (2013).
13. R. Bruck and O. L. Muskens, "Plasmonic nanoantennas as integrated coherent perfect absorbers on SOI waveguides for modulators and all-optical switches," Opt. Express **21**(23), 27652–27661 (2013).
14. R. R. Grote, J. B. Driscoll, and R. M. Osgood, Jr., "Integrated optical modulators and switches using coherent perfect loss," Opt. Lett. **38**(16), 3001–3004 (2013).
15. A. Mock, "Low-power all-optical switch based on time-reversed microring laser," IEEE Photonics J. **4**(6), 2229–2235 (2012).

16. W. Li, B. Chen, C. Meng, W. Fang, Y. Xiao, X. Li, Z. Hu, Y. Xu, L. Tong, H. Wang, W. Liu, J. Bao, and Y. R. Shen, "Ultrafast all-optical graphene modulator," Nano Lett. **14**(2), 955–959 (2014).
17. J. A. Dionne, K. Diest, L. A. Sweatlock, and H. A. Atwater, "PlasMOStor: a metal-oxide-Si field effect plasmonic modulator," Nano Lett. **9**(2), 897–902 (2009).
18. B. Jalali and S. Fathpour, "Silicon photonics," J. Lightwave Technol. **24**(12), 4600–4615 (2006).
19. W. M. Green, M. J. Rooks, L. Sekaric, and Y. A. Vlasov, "Ultra-compact, low RF power, 10 Gb/s silicon Mach-Zehnder modulator," Opt. Express **15**(25), 17106–17113 (2007).
20. S. I. Bozhevolnyi, V. S. Volkov, E. Devaux, J.-Y. Laluet, and T. W. Ebbesen, "Channel plasmon subwavelength waveguide components including interferometers and ring resonators," Nature **440**(7083), 508–511 (2006).
21. D. Pacifici, H. J. Lezec, and H. A. Atwater, "All-optical modulation by plasmonic excitation of CdSe quantum dots," Nat. Photonics **1**(7), 402–406 (2007).
22. J. Gosciniak, S. I. Bozhevolnyi, T. B. Andersen, V. S. Volkov, J. Kjelstrup-Hansen, L. Markey, and A. Dereux, "Thermo-optic control of dielectric-loaded plasmonic waveguide components," Opt. Express **18**(2), 1207–1216 (2010).
23. Z. Wu, R. L. Nelson, J. W. Haus, and Q. Zhan, "Plasmonic electro-optic modulator design using a resonant metal grating," Opt. Lett. **33**(6), 551–553 (2008).
24. A. Melikyan, N. Lindenmann, S. Walheim, P. M. Leufke, S. Ulrich, J. Ye, P. Vincze, H. Hahn, T. Schimmel, C. Koos, W. Freude, and J. Leuthold, "Surface plasmon polariton absorption modulator," Opt. Express **19**(9), 8855–8869 (2011).
25. J. Park, K.-Y. Kim, I.-M. Lee, H. Na, S.-Y. Lee, and B. Lee, "Trapping light in plasmonic waveguides," Opt. Express **18**(2), 598–623 (2010).
26. J. Park, H. Kim, I.-M. Lee, S. Kim, J. Jung, and B. Lee, "Resonant tunneling of surface plasmon polariton in the plasmonic nano-cavity," Opt. Express **16**(21), 16903–16915 (2008).
27. T. Chung, S.-Y. Lee, E. Y. Song, H. Chun, and B. Lee, "Plasmonic nanostructures for nano-scale bio-sensing," Sensors (Basel) **11**(11), 10907–10929 (2011).
28. A. Yariv, "Universal relations for coupling of optical power between microresonators and dielectric waveguides," Electron. Lett. **36**(4), 321–322 (2000).
29. T. Søndergaard, J. Jung, S. I. Bozhevolnyi, and G. Della Valle, "Theoretical analysis of gold nano-strip gap plasmon resonators," New J. Phys. **10**(10), 105008 (2008).
30. M. J. Weber, *Handbook of Optical Materials* (CRC Press, 2003), Chap. 4–2.
31. J. A. Nelder and R. Mead, "A simplex method for function minimization," Comput. J. **7**(4), 308–313 (1965).

1. Introduction

Efficient light absorption is a key issue in a wide range of technologies such as displays, photovoltaic cells, photo-detection, electromagnetic shielding, novel heat transfer, and ultra-fast photonic modulation [1, 2]. Perfect light absorbers refer to any structure of which working process causes light to be absorbed completely in a certain circumstance, so that there is no scattered light radiated from the structure. In general, the perfect absorption of light can be accomplished by satisfying the critical coupling condition of light into the structure, which means that the coupling ratio of the resonant structure is equal to the loss of the structure. However, such condition is fragile to be maintained, so its practical implementation is challenging.

Numerous methods have been proposed for achieving perfect light absorption for last years. For instance, some metasurface structures have been introduced as perfect absorbers [3–6]. Coherent perfect absorber (CPA) is one of promising approaches for perfect light absorption. The theory of CPA is that, if the coherence time of light is sufficiently long, an ideal extinction ratio, approaching to infinity, can be obtained by modulating the phase difference between the interfering light waves on an absorptive material. Since the first proposal of two-channel CPA made in a silicon thin film [7, 8], researchers have extensively studied its fundamental mechanisms and enlarged functionalities of sophisticated structures [9–11]. Also, the CPA in waveguides via plasmonic resonance has been addressed in depth [12–15]. It was shown that optimally engineered gold rod trimers on the silicon waveguide produced CPA at telecommunication wavelength, however, it was revealed that the width reduction of the waveguide is fundamentally limited. The CPA structure with nano-scale footprint working in the near-IR band can be an elementary block for nanoscale photonic integrated circuits, but not many reports on the nano-scale CPA structures at that wavelength band were provided [16–24].

#242203 Received 1 Jun 2015; revised 19 Jul 2015; accepted 4 Sep 2015; published 10 Sep 2015

In this paper, we present a design of ultra-small CPA-embedded plasmonic MIM waveguide structure that has the footprint of around 100 nm^2 and works in the near-IR band. It is shown that the control of the structural parameters of the embedded CPA can flexibly adjust the CPA resonance at any wavelength in the near-IR band from 1 μm to 1.6 μm. One consequence of our study is that, the use of the magnetic resonant CPA is crucial for positioning the CPA resonance in the near-IR band, while the conventional electric dipole resonant CPA is not appropriate for that purpose. This argument is verified through theoretical analysis.

This paper is organized as follows. In Section 2, the working principle of the proposed CPA is described. Section 3 elucidates the importance of implementing magnetic resonant CPA for accomplishing the design goal. In Section 4, the absorption characteristics of the proposed structure are analyzed and followed by the concluding remarks in Section 5.

2. Working principle of the proposed CPA

Figure 1(a) shows the proposed CPA structure embedded in a two-dimensional MIM plasmonic waveguide. The MIM plasmonic waveguide has a subwavelength-thick dielectric core, sandwiched by metal claddings, which is designed to forbid the propagation of the photonic modes. The MIM waveguide sustains two plasmonic modes, of which field distribution is evanescent both in metal and dielectric region. One of them is the magnetic field symmetric (fundamental) MIM mode, and the other is the anti-symmetric mode. Subwavelength thickness of the core is needed to obtain extreme confinement and it ensures that the anti-symmetric mode is cut-off or decayed much faster than symmetric one [25, 26]. Dimension of the proposed structure is chosen as not greater than 250 nm, thus we can assume that concerned mode is always magnetic field symmetric in this study. It is noteworthy that the symmetric MIM mode undergoes weak loss with propagation length more than 40 um in the considered near-IR region (1 μm–1.6 μm).

The CPA part consists of two parallel thin metal strips. Since we assume that only the fundamental MIM mode exists, this configuration can be effectively supposed to be a two-port system, where the input and output modes are the fundamental modes propagating towards and against the CPA, respectively. Moreover, by the mirror symmetry of the CPA structure with respect to the x -axis, the scattering matrix of the system can be written as:

$$\mathbf{S} = \begin{pmatrix} t & r \\ r & t \end{pmatrix}, U^{(o)} = \mathbf{S}U^{(i)}, \tag{1}$$

where r, t are complex reflection and transmission coefficients at the $x = 0$ surface, and the eigenvectors of the scattering matrix represent symmetrically incident MIM mode, $U^{(i)} = \begin{pmatrix} U_1^{(i)} & U_2^{(i)} \end{pmatrix}^{\mathrm{T}} = \begin{pmatrix} 1 & 1 \end{pmatrix}^{\mathrm{T}}$ and the anti-symmetrically incident MIM mode, $U^{(i)} = \begin{pmatrix} 1 & -1 \end{pmatrix}^{\mathrm{T}}$, respectively. In the analysis, we assume that the scattering process occurs at the center position $x = 0$. In practice, in order to obtain the effective scattering coefficients at $x = 0$, we calculate the scattering amplitudes at $x = \pm 1\mu\mathrm{m}$, the positions distant from the center of the plasmonic absorbing structure, and convert them to the scattering coefficients, r and t, at $x = 0$ with the compensation of propagating loss and phase retardation. This assumption does not harm the simulation results if the plasmonic absorbing structure is thin enough.

Meanwhile, plasmonic resonances of two parallel metal strips are hybridized by interacting identical resonant structure pair, as depicted in Fig. 1(b) [27]. When the distance between the metal strips is far enough, the resonant modes of two strips are degenerate in the resonance frequency ω, and the electric dipoles are induced in each metal strip. If the strips

#242203 Received 1 Jun 2015; revised 19 Jul 2015; accepted 4 Sep 2015; published 10 Sep 2015

are close enough to be optically coupled, the coupled resonant modes are well-separated in ω-domain – one is the electric-dipole resonance at higher frequency and the other is the magnetic-dipole resonance at lower frequency. Field radiations from those induced dipole moments are obviously different. For the case of magnetic dipole resonance, the current loop formed by oppositely flowing current induces magnetic field through the parallel metal strips structure, so that it scatters waves such that $U_1^{(o)} = U_2^{(o)}$, which means that bidirectional waves propagating against the structure are in-phase with respect to the magnetic field, but out-of-phase with respect to the electric field at the same distance from the structure. On the other hand, for the case of electric dipole resonance, the electric field is in-phase and the magnetic field is out-of-phase at the same distance from the structure. In this case, induced currents on metal strips are in the same directions and do not form any current loop component.

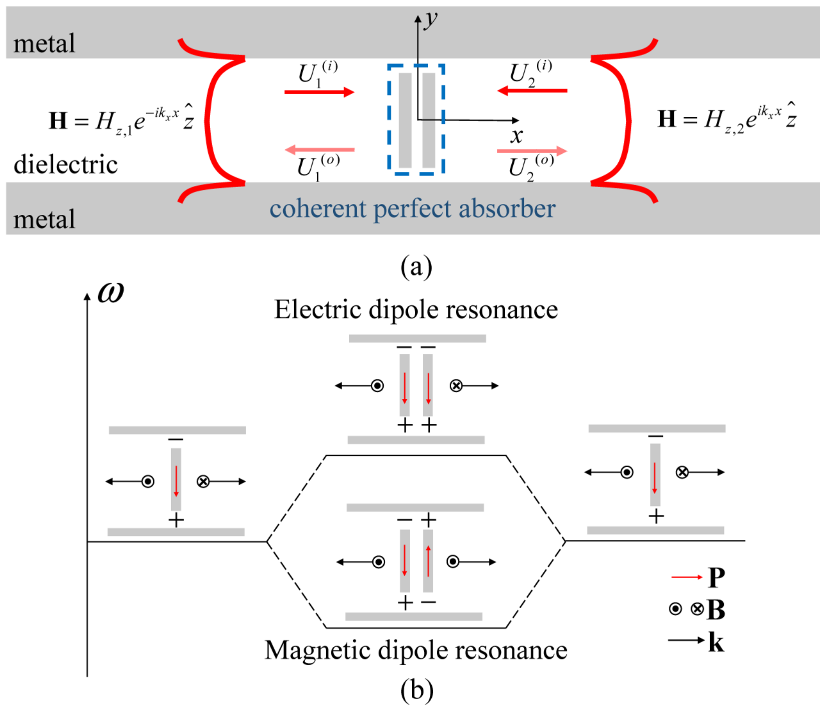

Fig. 1. (a) The proposed CPA embedded in an MIM plasmonic waveguide is depicted. Parallel metal strips absorb light via magnetic dipole resonance. Two metal strips should be close enough to hybridize their plasmonic resonances. (b) When the parallel metal strips embedded in the plasmonic waveguide are close enough, two resonant modes are hybridized into electric dipole resonance and magnetic dipole resonance, respectively. The two resonances are separated in the frequency domain (ω-axis). Polarization current (red arrows) and charge distribution (plus, minus sign) are indicated for each case.

According to the simple rule in the antenna theory that a good emitter is also a good receiver, it is expected that the proposed structure acts as a good absorber of symmetrically incident MIM modes ($U_1^{(i)} = U_2^{(i)}$) at the resonance frequency of magnetic dipole resonance. The amplitude of the induced magnetic dipole is proportional to the *z*-component of the magnetic field, penetrating through the current loop. On the other hand, since the electric-dipole resonant mode is well-separated in the frequency domain, the CPA absorbs little amount of energy of anti-symmetrically incident mode ($U_1^{(i)} = -U_2^{(i)}$) at the same frequency. We expect that optimized structure can show perfect absorption for symmetric incidence and

#242203 Received 1 Jun 2015; revised 19 Jul 2015; accepted 4 Sep 2015; published 10 Sep 2015

almost perfect transmission for anti-symmetric incidence. Such a high extinction property is desirable for the design of amplitude switching devices.

Mathematically, the perfect absorption condition corresponds to the condition that one of the eigenvalues of scattering matrix, **S**, is zero. According to Eq. (1), one of the perfect absorption conditions is $r = t$, and the other is $r = -t$. The first case needs to have electric dipole resonance, and the second case corresponds to the magnetic dipole resonance when thin dipole sheet is concerned as we can deduce it from Fig. 1(b).

We define a parameter $m = (r + t - 1)/2$ for the magnetic resonant CPA which is defined at $x = 0$ surface. It represents the relative amount of symmetrically scattered light. If the CPA condition meets with $r = -t$, m is equal to $-1/2$. This condition is equivalent to the critical coupling condition [28] where loss rate and coupling rate should be equal to absorb incident power perfectly. There are three key observations to understand this parameter: (i) m is proportional to the strength of induced magnetic dipole on the structure, (ii) the structure behaves as a simple harmonic oscillator, and (iii) the structure is passive. From (i) and (ii), the frequency dependence of m can be modeled as $m = m_0 / (1 + i(\omega - \omega_0)/\gamma)$, where m_0 is the relative amplitude of the symmetrically scattered light on resonance, γ is bandwidth or loss rate, and ω_0 is the resonance frequency. m_0 should be between -1 and 0 to satisfy (iii). For appropriate scattering amplitude, m_0 is equal to $-1/2$. Similarly, in the case of electric resonant CPA, the counterpart parameter of m, p, is defined by $p = (-r + t - 1)/2$. The coherent perfect absorption condition for the electric resonant CPA is obtained at $p = -1/2$.

The introduction of the parameters p, m and the relationship between r, t, p and m can be justified as follows. The total wave is assumed to be the superposition of incident wave and scattered wave. In the case of one-sided illumination, reflection coefficient r is equal to the relative amplitude of the scattered wave only and transmission coefficient t is sum of one and the relative amplitude of the scattered wave. Then there are two types of scattering process: electric dipole and magnetic dipole, the amplitudes of which are represented as p and m, respectively. If we set that the relative amplitude of the scattered wave propagating toward the same direction with the incident wave has plus sign, then the transmission and reflection coefficient in the magnetic field distribution are given by $t = 1 + p + m$, and $r = -p + m$, respectively. A simple algebra results in the representation of $m = (r + t - 1)/2$, and $p = (-r + t - 1)/2$.

As indicated in Fig. 1(b), the plasmonic hybridization puts the magnetic resonance energy to a lower energy level. Moreover, comparing the designs of electric dipole and magnetic dipole resonators working for a specific design wavelength, we can reasonably infer that the electric dipole resonance occurs with relatively long strip but the magnetic dipole resonance does with relatively short strip for the same resonance frequency, which relies on the fact that plasmonic resonance frequency of the structure is strongly dependent on the length of the strip. Thus, the use of magnetic dipole resonance is essential for the realization of CPA in the near-IR region within smaller footprint. We can also think about the high-order modes of plasmonic absorbing structure, which would influence the behavior of a single simple oscillator. However, the high-order modes of metal strips are originated from the hybridization of high-order modes of the single metal strip, which tend to live in high frequency region. Also, the coupling from the incident mode to high-order modes are effectively inhibited by transverse wavevector mismatch between the incident field and the resonant field [29]. Moreover, we can suppress these unwanted higher-order effects by choosing the length of the metal strips as small as possible, so that only electric and magnetic dipole resonance exist in the operating frequency region.

In Fig. 2(a), the structural parameters that we can tune for optimizing the structure are indicated. Au is chosen for the metal medium of both the waveguide and the CPA structure and its complex permittivity profile is obtained from the experimental data [30].

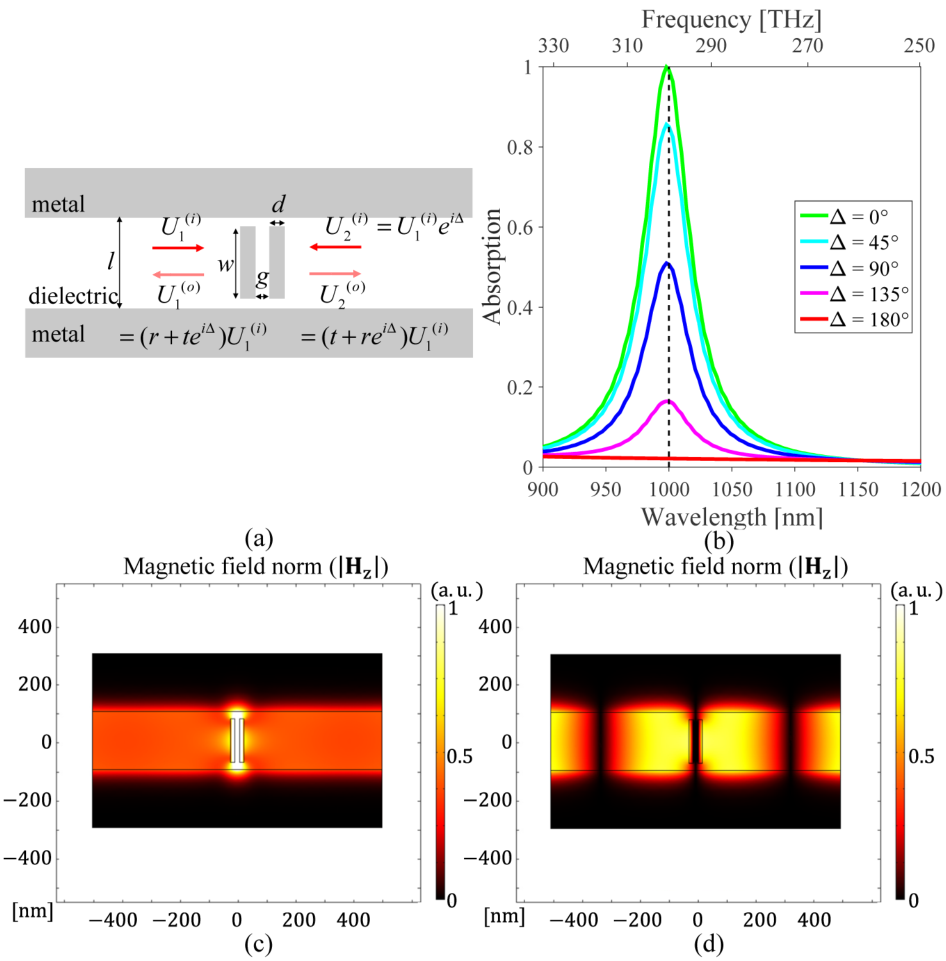

Fig. 2. (a) Structural parameters and scattering process of the proposed structure are depicted. (b) Absorption ratio of an optimized CPA structure against wavelength with different relative phase, Δ. Values of the parameters are $d = 15$ nm, $w = 150$ nm, $g = 16.5$ nm, and $l = 200$ nm. Magnetic field distribution of CPA structure for (c) symmetrically incident waves, $\Delta = 0$, and (d) anti-symmetrically incident waves, $\Delta = \pi$.

As depicted in Fig. 2(a), there are four parameters to be varied: the dielectric core thickness l, the length of the strips w the thickness of each strip d and the gap size g. To reduce the complexity of the parameter space, l is not used as an optimization target, but considered as a pre-determined value. The value of l should be smaller than the operating wavelength to ensure the cut-off of the photonic modes. Moreover, l has to be barely longer than w to enhance coupling ratio. The parameters, w, d and g are related to the on-resonance frequency of the magnetic dipole ω_m. Hence, setting the three parameters to

#242203 Received 1 Jun 2015; revised 19 Jul 2015; accepted 4 Sep 2015; published 10 Sep 2015

appropriate values can optimize the characteristics of the magnetic dipole resonance. w is almost solely dependent on the plasmon resonance of each metal strip. When gold is chosen for the metal media, it should be around 100 nm in order to make the resonances at the near-IR region. g determines the frequency separation between electric and magnetic dipole resonance by plasmonic hybridization. Since the separation should be large to retain high extinction ratio, it is preferred for g to be sufficiently small. Typical value of g is below 30 nm long for plasmonic hybridization. Lastly, d is tuned for coherent perfect absorption condition. As d increases, the structure scatters light more in a proportional way. However, it does not indicate that the absorption ratio is also proportional to d.

With the Nelder-Mead method [31], we have optimized the CPA structure. At target frequency ω_t, we have chosen for objective function as

$$f(l,w,g,d) = \left|m(\omega_t) + 1/2\right|^2, \tag{2}$$

which is aforementioned. If CPA condition lies on the parameter space, then its minimal value has to be zero. As a result, we have obtained the optimal structural parameters, $w = 150$ nm, $d = 15$ nm, and $g = 16.5$ nm and achieved the absorption ratio above 0.999 at $\omega_t = 1\mu\text{m}$ wavelength. In the optimization and analysis, we employed the commercial software COMSOL Multiphysics.

As shown in Fig. 2(b), when the phase difference of incident counter-propagating waves, Δ, is changed from 0 to π, then absorption ratio of CPA at the on-resonance frequency is modulated from the maximum value 1 to the minimum value near 0. The transmitted modes are represented by

$$U_{1(2)}^{(o)} = \left(r + te^{\pm i\Delta}\right)U_{1(2)}^{(i)}. \tag{3a}$$

Then, the absorption ratio can be simply formulated:

$$A = \cos^2\frac{\Delta}{2} + A_0\sin^2\frac{\Delta}{2} \approx \cos^2\frac{\Delta}{2}, \tag{3b}$$

where A_0 is the absorption ratio when plasmonic waves are incident anti-symmetrically. This value can be ignored if g is small enough.

Not surprisingly, Fig. 2(b) depicts the dependence of the absorption ratio on the phase difference in accordance to Eq. (3). In Figs. 2(c)-2(d), the magnetic field distributions in the CPA structure at $\Delta = 0$ and at $\Delta = \pi$ are shown, respectively. The symmetrically incident MIM modes ($\Delta = 0$) produces the magnetic field distribution interfering constructively at the CPA structure ($x = 0$), while the anti-symmetrical incidence ($\Delta = \pi$) induces destructive interference and allows visible standing wave pattern formation in MIM waveguide. This simulation result is consistent with the aforementioned qualitative analysis.

3. Comparison of electric and magnetic resonant CPA in MIM structure

As assumed in the previous section, the magnetic resonant dipole m is modeled as a simple harmonic oscillator. Then, the value of m can have a typical trajectory of circle as graphically shown in Fig. 3(a), having the radius of $m_0/2$ and centered at $(-m_0/2, 0)$. When the symmetrical MIM mode input is applied, the amplitudes of out-coupled light from the CPA are given by $U_1^{(o)} = U_2^{(o)} = (r+t)U_1^{(i)}$, or $U_1^{(o)} = U_2^{(o)} = \left(m(\omega) - (-1/2)\right)U_1^{(i)}$. In Fig. 3(a), the ratio of transmitted power over the total power is interpreted as the square of the distance between $(-1/2, 0)$ and $m(\omega)$. The CPA condition is achieved if the distance becomes zero,

#242203 Received 1 Jun 2015; revised 19 Jul 2015; accepted 4 Sep 2015; published 10 Sep 2015

which can only be satisfied when the trajectory of $m(\omega)$ meets the point $(-1/2, 0)$, i.e. $m_0 = 1/2$ (red line in Fig. 3(a)). Also, there are blue line and green line that indicate under-coupled case and over-coupled case, respectively.

As an example of tuning m_0, Fig. 3(b) shows the extracted complex values of m from the full-field simulation results for various gap size of the CPA. The circular loops of the calculated m indicate that the proposed CPA is well matched to the simple harmonic oscillator model, and they also show that the value of m_0 can be tuned by changing the structural parameters properly. In particular, it is seen that the amount of the resonant hybridization can be arbitrarily tuned by changing the gap between the metallic strips, g.

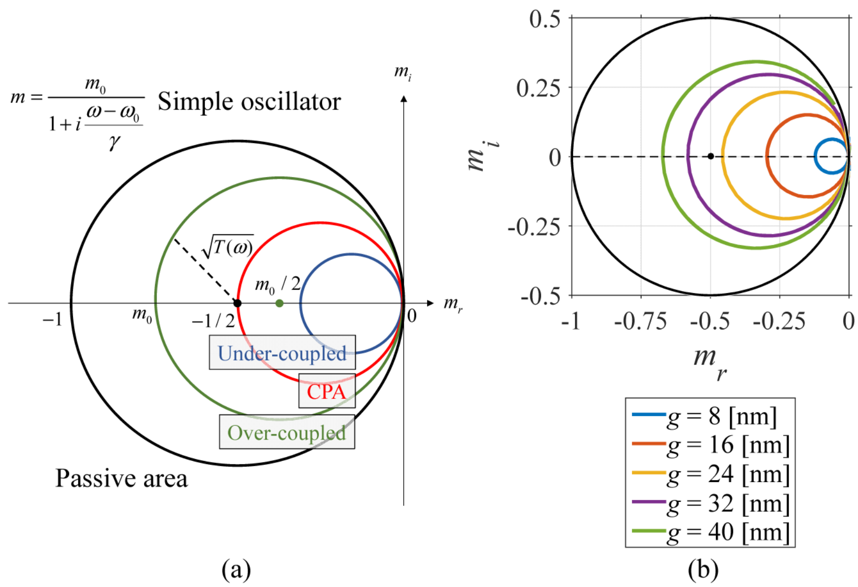

Fig. 3. Manipulating the values of geometric parameters changes the scattering matrix S. Frequency dependence of the complex-valued parameter m: (a) schematic of the trajectory of the parameter, (b) numerical results derived from five different structures. The other parameters are fixed at $d = 10$ nm, $w = 160$ nm, and $l = 200$ nm.

For comparison, we carry out the same analysis on the parameter, p, which stands for the complex amplitude of the anti-symmetrically scattered light in the electric resonant CPA. Figure 4(a) shows a single strip embedded in the same plasmonic MIM waveguide. In Fig. 4(b), the absorption efficiency for various d is plotted as a function of wavelength, which depicts that the single strip cannot absorb light effectively irrespective to the thickness, d. As seen in Fig. 4(c), the single-strip structure, i.e. electric resonant structure, is highly over-coupled. If we have to achieve perfect absorption by electric dipole resonance at any cost, we must adopt 1 nm order thick metal strip as we can guess it from Fig. 4(c). This case is very unrealistic in various ways, size-dependent plasmonic loss, quantum effect, and etc.

We can also consider the electric dipole resonance of two metal strips. However, it is blue-shifted for reducing the distance d, so that it is not appropriate for near-IR operation with constraint of compactness. Moreover, electric dipole resonance is still in over-coupling regime no matter when the plasmonic structure is hybridizing two coupled metallic strips. Thus, electric dipole resonance is not considered as the plasmonic absorbing structure for low-loss waveguiding in near-IR region and for the use of critical coupling scheme.

The observation from the comparison of magnetic and electric dipole resonances tells that the use of magnetic dipole resonance for CPA is superior to electric dipole resonance for two reasons. Firstly, the magnetic resonance structure can be gently tuned with the amount of plasmonic hybridization so that appropriate scattering amplitude for achieving CPA condition is achieved. Secondly, the resonance peak of the magnetic dipole resonance can be flexibly adjusted from the resonance of single plasmonic structure at the near-IR region, so that the resonance is easily located at any wavelength of near-IR region in ultra-compact MIM waveguide structure.

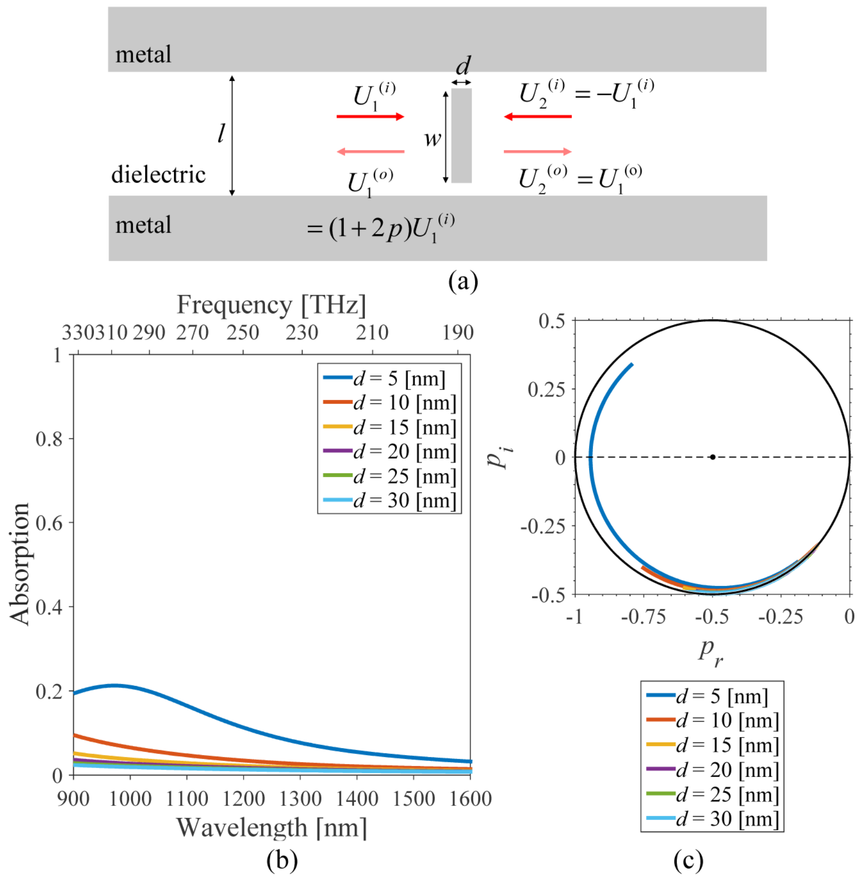

Fig. 4. Numerical analysis on a single strip embedded in a MIM waveguide with anti-symmetrically incident light: (a) structural parameters (b) the absorption spectra of a single strip and (c) the corresponding trajectory of the complex-valued parameter p. The other parameters are fixed at $w = 150$ nm and $l = 200$ nm.

4. Analysis of CPA characteristics

In this section, the dependence of the CPA spectra on the structural parameters are numerically analyzed. In this calculation, the absorption ratio is compensated to be not overestimated by the waveguide propagation loss. In Fig. 5(a), it is seen that the absorption spectrum is red-shifted as the length of strips grows and the peak value at on-resonance frequency is almost independent of w. The spectrum shifting seems to be ascribed to the Fabry-Perot resonance. However, Fig. 5(b) presents that the thickness of metal strips, d , can change both the resonance frequency and the peak value at on-resonance. The aspect ratio of plasmonic structure affects depolarization factor, so on-resonance frequency is blue-shifted

#242203 Received 1 Jun 2015; revised 19 Jul 2015; accepted 4 Sep 2015; published 10 Sep 2015

by growing d. Also, increasing d causes the enhancement of induced current on the metal strips, so that m_0 grows proportional to d. Absorption ratio is then quadratic with d. The peak value is maximum at the certain structural parameter, which satisfies the condition, $m_0 = -1/2$. In Fig. 5(c), we can see that the resonance frequency is blue-shifted with g. Simultaneously, the scattering amplitude, m, increases with g because the magnetic dipole moment is proportional to the area of circular current loop. Finally, Fig. 5(d) shows the absorption spectra of various CPA structures which are optimized for different on-resonance frequencies, from 1μm to 1.6μm. The design results show that the CPA condition in the proposed structure can be fit for broad range in near-IR band.

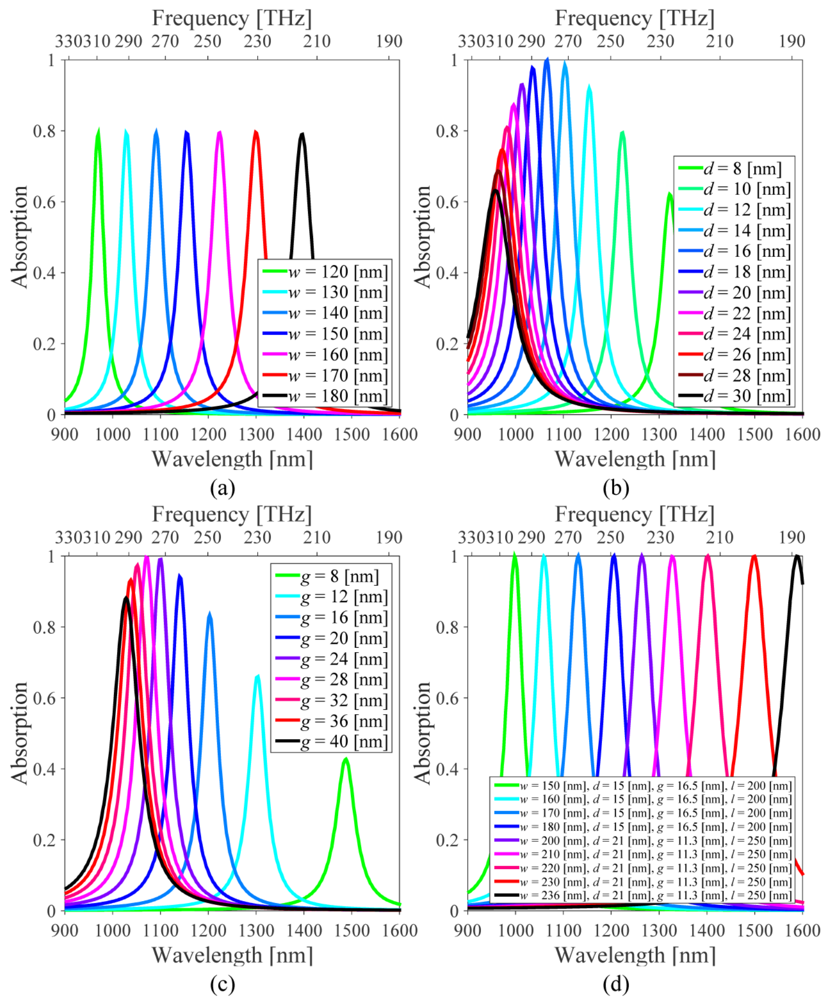

Fig. 5. Absorption spectra of symmetrically incident waves in the proposed structure with varying (a) w, (b) d and (c) g. l is fixed at 200 nm. The other parameters are fixed at (a) $d = 10\text{nm}$, $g=15\text{nm}$, (b) $g = 15$ nm, $w = 160$ nm, and (c) $w = 160$ nm, $d = 10$ nm. (d) Absorption spectra for various CPA structures with operating wavelength between 1 μm (green line) and 1.6 μm (black line).

#242203 Received 1 Jun 2015; revised 19 Jul 2015; accepted 4 Sep 2015; published 10 Sep 2015

5. Conclusion

In conclusion, we have proposed ultra-compact near-IR CPA based on plasmonic MIM waveguide and describes the design procedure and the analysis on the CPA characteristics. The proposed CPA consists of parallel metal strips, which give a magnetic dipole resonance. It absorbs counter-propagating fundamental MIM plasmonic modes efficiently when magnetic field interferes constructively, which leads to produce ultra-compact near-IR CPA with excellent extinction ratio. The proposed CPA can also be extended to give an effective compact amplitude modulation scheme with active phase modulation. Although we consider two-dimensional structure for convenience, the extension to a 3D waveguide would be resolved through the similar analysis with an additional consideration of scattering into the free-space and additional optimization process, as discussed in other literature [13].

Acknowledgment

This research was supported by Global Frontier Program through the National Research Foundation of Korea (NRF) funded by the Ministry of Science, ICT & Future Planning (2014M3A6B3063710).